

# Entropy measurement of a strongly correlated quantum dot

Tim Child,<sup>1,2,\*</sup> Owen Sheekey,<sup>1,2</sup> Silvia Lüscher,<sup>1,2</sup> Saeed Fallahi,<sup>3,4,5</sup> Geoffrey C. Gardner,<sup>4,5,6</sup> Michael Manfra,<sup>3,4,7,6,5</sup> Yaakov Kleeorin,<sup>8</sup> Yigal Meir,<sup>9,10</sup> and Joshua Folk<sup>1,2,†</sup>

<sup>1</sup>Stewart Blusson Quantum Matter Institute, University of British Columbia, Vancouver, British Columbia, V6T1Z4, Canada

<sup>2</sup>Department of Physics and Astronomy, University of British Columbia, Vancouver, British Columbia, V6T1Z1, Canada

<sup>3</sup>Department of Physics and Astronomy, Purdue University, West Lafayette, Indiana, USA

<sup>4</sup>Birck Nanotechnology Center, Purdue University, West Lafayette, Indiana, USA

<sup>5</sup>Microsoft Quantum Lab Purdue, Purdue University, West Lafayette, Indiana, USA

<sup>6</sup>School of Materials Engineering, Purdue University, West Lafayette, Indiana, USA

<sup>7</sup>School of Electrical and Computer Engineering,  
Purdue University, West Lafayette, Indiana, USA

<sup>8</sup>Center for the Physics of Evolving Systems, University of Chicago, Chicago, IL, 60637, USA

<sup>9</sup>Department of Physics, Ben-Gurion University of the Negev, Beer Sheva 84105, Israel

<sup>10</sup>The Ilse Katz Institute for Nanoscale Science and Technology,  
Ben-Gurion University of the Negev, Beer Sheva 84105, Israel

(Dated: October 28, 2021)

The spin 1/2 entropy of electrons trapped in a quantum dot has previously been measured with great accuracy, but the protocol used for that measurement is valid only within a restrictive set of conditions. Here, we demonstrate a novel entropy measurement protocol that is universal for arbitrary mesoscopic circuits and apply this new approach to measure the entropy of a quantum dot hybridized with a reservoir, where Kondo correlations dominate spin physics. The experimental results match closely to numerical renormalization group (NRG) calculations for small and intermediate coupling. For the largest couplings investigated in this work, NRG predicts a suppression of spin entropy at the charge transition due to the formation of a Kondo singlet, but that suppression is not observed in the experiment.

Entropy is a powerful tool for identifying exotic quantum states that may be difficult to distinguish by more standard metrics, like conductance. For example, bulk entropic signatures in twisted bilayer graphene indicate that carriers in some phases with metallic conductivity retain their local moments, as would normally be associated with a Mott insulator [1–3]. Entropy has also been proposed as a tell-tale characteristic of isolated non-abelian quasiparticles, whether Majorana modes in a superconductor [4, 5] or excitations of a fractional quantum Hall state [6], distinguishing them from more conventional (abelian) analogs.

Quantifying the entropy of single quasiparticles is challenging due to the small signal size, of order  $k_B$ , but first steps in this direction have been made in recent years [7, 8]. Ref. 7 employed Maxwell relations to measure the  $k_B \ln 2$  spin entropy of a single electron confined to a quantum dot (QD) in GaAs via the temperature-induced shift of a Coulomb blockade charge transition. That approach relied on the assumption of weak coupling between the QD and the reservoirs, in order to fit based on the specific charging lineshape known for that regime. In that weak-coupling regime, spin states are pristine enough to serve as spin qubits [9–15] but the underlying physics is very simple.

The approach in Ref. 7 is not applicable to a broad class of mesoscopic devices [16], which limits its value in probing the complex Hamiltonians that may be implemented in such systems. For example, a single-impurity Kondo effect is realized when the localized spin

is strongly coupled to a reservoir [17, 18]. Recently, more complicated structures including multiple dots have been engineered to host multi-channel Kondo states [19, 20], a three-particle simulation of the Hubbard model [21], and more. Entropy measurements made on any of these systems would offer a significant advance in understanding, but are not yet possible.

Here, we develop a universal protocol for mesoscopic entropy measurement that forgoes the simplifying assumptions of Ref. 7, then apply it to investigate how Kondo correlations due to hybridization with a reservoir affect the entropy of the first electron entering a quantum dot. The new approach is based on a different Maxwell relation, expressed in integral form,

$$\Delta S_{\mu_1 \rightarrow \mu_2} = \int_{\mu_1}^{\mu_2} \frac{dN(\mu)}{dT} d\mu, \quad (1)$$

that provides access to the entropy change,  $\Delta S$ , with chemical potential  $\mu$ , based on measurements of the change in quantum dot occupation,  $N$ , with temperature,  $T$  [5].

When the coupling,  $\Gamma$ , between dot and reservoir is weak ( $\Gamma \ll k_B T$ ), the characteristic temperature of Kondo correlations is much less than the experimental temperature,  $T_K \ll T$ , and the measurement matches well to single-particle approximations. When  $\Gamma \gtrsim k_B T$ , the onset of entropy as the electron enters the dot is strongly modified, and the data are consistent with numerical renormalization group (NRG) calculations [22, 23] that include the effect of Kondo correla-

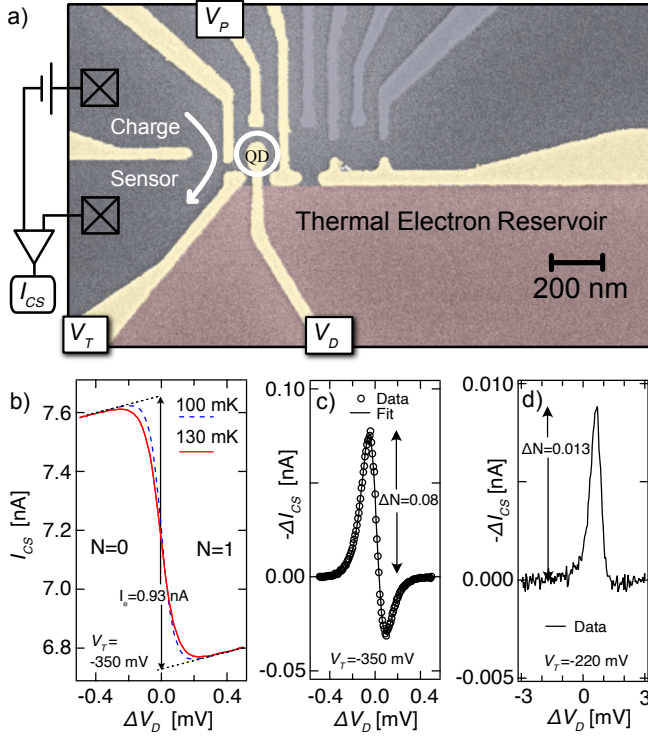


FIG. 1. a) Scanning electron micrograph (colour added) of the device. Electrostatic gates (gold) define the circuit in a 2D electron gas. Grey gates were unused and remained grounded. Squares represent ohmic contacts to the 2DEG. The thermal electron reservoir (red) was alternated between base and elevated temperatures. b) Current through the charge sensor for the  $0 \rightarrow 1$  charge transition in a weakly coupled regime, separated into the unheated (100 mK) and heated (130 mK) parts of the interlaced measurement [24], showing  $N = 0 \rightarrow 1$  step height  $I_e$ . c, d) Change in  $I_{CS}$  from 100 to 130 mK, for weak (c) and strong (d) coupling between QD and reservoir. c) includes fit to weakly-coupled theory, yielding  $\Delta S_{\text{fit}} = (1.02 \pm 0.01)k_B \ln 2$ .

tions. For  $\Gamma \gg k_B T$ , a persistent shift appears between data and NRG, calling for further investigation.

Measurements were performed on a circuit (Fig. 1a) defined by voltages applied to electrostatic gates over a GaAs 2D electron gas [25], similar in functionality to that in Ref. 7, with improvements made in the design and entropy measurement protocol [24]. The circuit includes the QD, a charge sensing quantum point contact, and an electron reservoir that can be rapidly Joule-heated above the chip temperature  $T$  to an elevated  $T + \Delta T$ . Both  $T$  and  $T + \Delta T$  were calibrated by fitting to thermally broadened charge transitions; except where noted,  $T = 100$  mK with  $\Delta T \sim 30$  mK. Coupling between the QD and the thermal reservoir is via a single tunnel barrier, with transmission controlled by  $V_T$ .

Coarse adjustments in the QD energy level were made using gate voltage  $V_P$ , with fine adjustments controlled by  $V_D$ . In practice,  $V_P$  and  $V_D$  tune the chemical poten-

tial as it enters into Eq. 1 by adjusting the difference in energy between  $\mu$  in the reservoir and the energy needed to add an electron to the dot [16]. Throughout this paper we report  $V_D$  with respect to the midpoint of the charge transition,  $\Delta V_D \equiv V_D - V_D(N = 1/2)$ .

$N$  was monitored via the current,  $I_{CS}$ , through the nearby charge sensor [9], which was biased with a DC voltage between 50 and 300  $\mu$ V. Fig. 1b illustrates weakly coupled  $N = 0 \rightarrow 1$  transitions at two different temperatures, with  $I_e$  defined as the net drop in  $I_{CS}$  across the transition due to the addition of  $1e$  charge to the dot. Measurements at the two temperatures were interlaced by alternated Joule heating of the reservoir at 25 Hz to reduce the impact of charge instability, then averaged over several sweeps across the charge transition, see Ref. 25.

Figure 1c shows the difference between the weakly-coupled transitions in Fig. 1b,  $\Delta I_{CS}(V_D) \equiv I_{CS}(T + \Delta T, V_D) - I_{CS}(T, V_D)$ . Note that  $-\Delta I_{CS}$  is plotted instead of  $I_{CS}$  in order to connect visually with  $\Delta N$ , which increases when  $I_{CS}$  decreases. As in Ref. 7, the lineshape of  $\Delta I_{CS}(V_D)$  in Fig. 1c may be fit to a non-interacting theory for thermally-broadened charge transitions to extract the change in entropy across the transition,  $\Delta S_{\text{fit}}$ , not requiring calibration factors or other parameters (see Ref. 7 for details). For the data in Fig. 1c, this yields  $\Delta S_{\text{fit}} = (1.02 \pm 0.01)k_B \ln 2$ , where the uncertainty reflects standard error among 5 consecutive measurements at slightly different  $V_T$ . The limitation of this approach is illustrated by the very different lineshape in Fig. 1d, reflecting the  $0 \rightarrow 1$  transition when the QD is strongly coupled to the reservoir and Kondo correlations begin to play a role. Fitting to thermally-broadened theory would yield a meaningless  $\Delta S_{\text{fit}} > 10k_B \ln 2$  for the spin-1/2 electron.

The different lineshapes of  $\Delta I_{CS}(V_D)$  in Figs. 1c and d can be understood as representing two temperature regimes for the Kondo system consisting of a spin-1/2 electron coupled to a reservoir. Fig. 1c represents the high temperature limit, with  $T_K \ll T$  throughout the transition. Fig. 1d represents an intermediate regime, where the  $\mu$ -dependent Kondo temperature crosses over from  $T_K > T$  at the transition to  $T_K \ll T$  deep in the  $N=1$  state.

The integral approach in Eq. 1 requires no assumptions of weak coupling, interactions, or other characteristics of the quantum state, enabling a quantitative investigation of the crossover between the regimes represented in Figs. 1c and d. Furthermore, evaluating Eq. 1 provides a measurement of  $\Delta S(\mu)$  across the charge transition, rather than just comparing  $N = 0$  to  $N = 1$  values. To evaluate Eq. 1 from experimental data,  $dN(\mu)/dT$  is approximated by the ratio  $\Delta N(V_D)/\Delta T = -\Delta I_{CS}(V_D)/(I_e \Delta T)$ , with  $\Delta T$  expressed in units of gate voltage using the corresponding lever arm [25] so that the integral may be evaluated over  $V_D$  giving  $S(V_D)$ .

We begin by confirming the integral approach in the

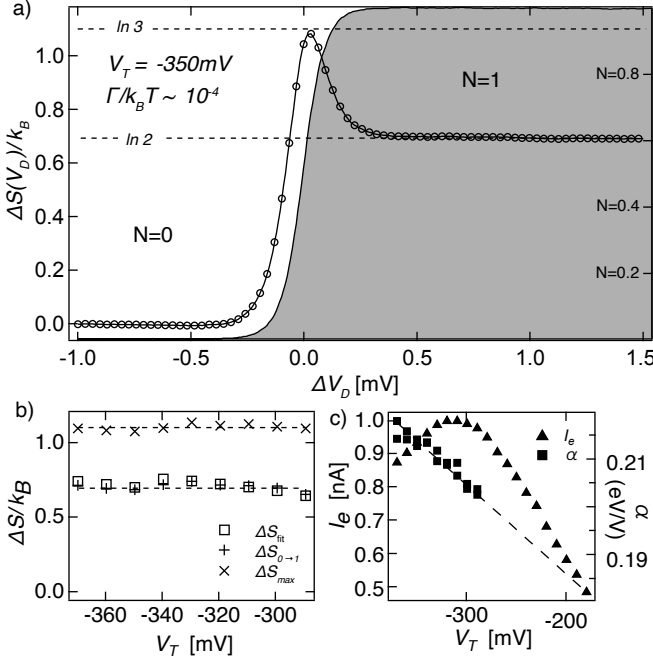


FIG. 2. a) Change of  $S$  in the QD across the  $N = 0 \rightarrow 1$  transition, obtained by integrating  $\Delta I_{CS}(V_D)$  (Fig. 1c) following Eq. 1. Dot occupation across the transition is shown in grey. Data obtained in the weakly coupled limit,  $V_T = -350$  mV corresponding to  $\Gamma/k_B T \sim 1 \times 10^{-4}$ .  $\Delta S_{0 \rightarrow 1} = (0.99 \pm 0.02)k_B \ln 2$  is the net change  $\Delta S$  across the complete transition. b) Comparison of  $\Delta S_{\text{fit}}$ ,  $\Delta S_{0 \rightarrow 1}$ , and  $\Delta S_{\text{max}}$  (see text) for  $V_T$  covering approximately  $10^{-5} < \Gamma/k_B T < 10^{-1}$ . c) Variation of charge step  $I_e$  and lever arm  $\alpha$ , measured independently over the full range of  $V_T$  explored in this experiment. Dashed line: extrapolation of  $\alpha$  into the strongly-coupled regime where it cannot be measured directly.

weakly-coupled regime, where the physics is simple. Fig. 2a shows the entropy change across the  $N = 0 \rightarrow 1$  charge transition for  $\Gamma \ll k_B T$ , calculated from the data in Fig. 1b using Eq. 1. The resulting  $\Delta S(\mu)$  indicates that the change in dot entropy is non-monotonic as the first electron is added, reaching a  $k_B \ln 3$  peak before settling to  $k_B \ln 2$ . The  $k_B \ln 3$  peak just above  $\Delta V_D = 0$  reflects a combination of charge and spin degeneracy on the dot in the middle of the charge transition, with three possible microstates  $\{|N = 0\rangle, |N = 1, \uparrow\rangle, |N = 1, \downarrow\rangle\}$  all equally probable. Charge degeneracy is gone after the transition, but spin degeneracy remains, leaving two possible microstates  $\{|N = 1, \uparrow\rangle, |N = 1, \downarrow\rangle\}$ . The net change in entropy from beginning to end,  $\Delta S_{0 \rightarrow 1} = (0.99 \pm 0.02)k_B \ln 2$ , is nearly identical to the  $\Delta S_{\text{fit}} = (1.02 \pm 0.01)k_B \ln 2$  from Fig. 1c, despite very different sources of error for the two approaches.

Figure 2b compares the fit and integral approaches for weakly-coupled charge transitions covering four orders of magnitude in  $\Gamma$ , with the coupling tuned by  $V_T$  (see Fig. 3b inset for calibration of  $\Gamma$ ). The consistency be-

tween  $\Delta S_{0 \rightarrow 1}$  and  $\Delta S_{\text{fit}}$ , and the fact that  $\Delta S_{\text{max}}$  remains  $k_B \ln 3$ , over the full range of weakly-coupled  $V_T$  confirms the accuracy of the integral approach. Small deviations from  $\Delta S_{0 \rightarrow 1} = \Delta S_{\text{fit}} = k_B \ln 2$ , such as that seen around  $V_T = -330$  mV, are repeatable but sensitive to fine-tuning of all the dot gates; we believe they are due to extrinsic degrees of freedom capacitively coupled to the dot occupation, such as mobile dopants in the GaAs heterostructure.

After confirming the accuracy of Eq. 1 in the weakly coupled regime, we turn to the regime  $\Gamma \gtrsim k_B T$  ( $V_T > -280$  mV), where the influence of hybridization and Kondo correlations is expected to emerge. Fig. 3 shows the crossover from  $\Gamma \ll k_B T$  to  $\Gamma \gg k_B T$ , illustrating several qualitative features. The  $k_B \ln 3$  peak in  $\Delta S(\mu)$  decreases with  $\Gamma$ , until no excess entropy is visible at the charge degeneracy point for  $\Gamma/k_B T \gtrsim 5$  (Figs. 3a). This suppression of the entropy associated with charge degeneracy originates from the broadening by  $\Gamma$  of the  $N = 1$  level due to hybridization with the continuous density of states in the reservoir [5]. At the same time, the total entropy change  $\Delta S_{0 \rightarrow 1}$  remains  $\sim k_B \ln 2$  over the entire range of  $\Gamma$  explored in this experiment, reflecting the entropy of the spin-1/2 electron trapped in the QD.

As analytical solutions do not exist for a spinful QD outside of the weakly coupled regime, we turn to NRG calculations as a comparison to measurement[22, 23]. NRG simulations yield  $N$  as a function of both  $T$  and  $\epsilon_0$ , where  $-\epsilon_0$  is the depth of the dot level below the reservoir potential. From  $N(T, \epsilon_0)$ ,  $dN/dT$  and therefore  $\Delta S$  may be extracted via Eq. 1. In order to make a direct comparison with the experiment,  $\Delta \epsilon_0 \equiv \epsilon_0 - \epsilon_0(N = 1/2)$  is defined like  $\Delta V_D$ , centred with respect to the charge transition. NRG parameters are calibrated to match those in the measurements by aligning the occupation  $N(\Delta \epsilon_0)$  with the measured  $N(\Delta V_D)$ [25], from which the appropriate  $\Gamma/T$  calculation may be selected and the precise connection between  $\Delta \epsilon_0$  with  $\Delta V_D$  is ensured. As seen in Fig. 3b, the data/theory agreement is perfect in terms of dot occupation, within the experimental resolution, giving confidence that measured and calculated  $\Delta S$  may be compared directly.

The calculations in Fig. 3c illustrate NRG predictions for  $\Delta S(\epsilon_0)$  over the range of  $\Gamma$  accessible in our measurements. Matching the data, the peak in entropy due to charge degeneracy is suppressed as  $\Gamma$  increases above  $\Gamma \gtrsim k_B T$ , while the net entropy change across the transition remains  $k_B \ln 2$ . At the same time, a clear qualitative difference between data and NRG is the shift to the right seen in NRG curves for higher  $\Gamma$  (Fig. 3c), but not observed in the measurements (Fig. 3a). This relative shift of NRG with respect to data is not explained by an offset of  $\Delta \epsilon_0$  with respect to  $\Delta V_D$ , as the two are aligned by the occupation data (Fig. 3b).

At first glance, the shift of NRG curves to the right may seem strange: why would the emergence of  $k_B \ln 2$

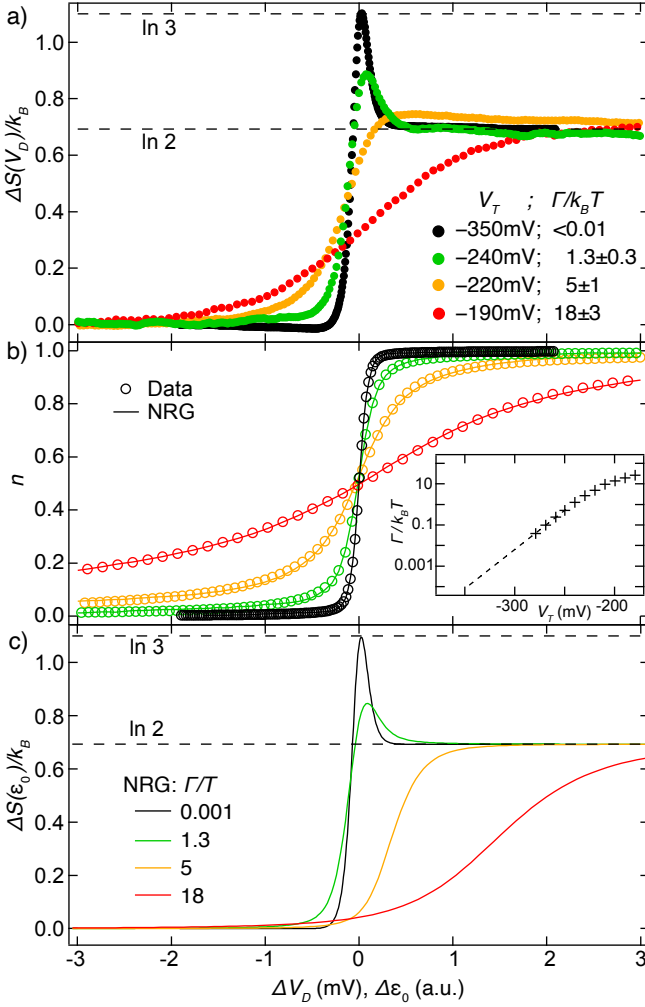


FIG. 3. Evolution of  $S(\mu)$  from the weak (black) to strong (red) coupling regimes, comparing data (panel a) to NRG calculations (panel c). Measurements of occupation across the charge transition are fit to NRG (panel b), leaving no free fit parameters for the  $S(\mu)$  calculation. Panel b inset: Coupling strength of the QD to the reservoir,  $\Gamma/k_B T$ , extracted from fits, across the full range of  $V_T$ . Values  $\Gamma/k_B T \ll 1$  cannot be measured directly and are extrapolated (dashed line).

entropy in the dot be delayed until after the electron is mostly localized in the dot? This behaviour is explained by the virtual exchange interactions underlying the Kondo effect, which form a quasi-bound singlet state between the localized spin and a cloud of delocalized spin for temperatures below  $T_K$ . This results in a state with no magnetic moment [26] and, in the case of a single-electron QD, zero entropy.

$T_K$  is largest in the middle of the charge transition [27], then suppressed exponentially by  $\epsilon_0$ , with functional form  $T_K \propto e^{\pi\epsilon_0(\epsilon_0 - U)/(\Gamma U)}$  far from the transition centre [27] where  $U$  represents the QD charging energy. For the present device geometry,  $\Delta I_{CS}$  collapses with  $\Gamma$ , limiting the strength of the coupling in the measurement to

$\Gamma/k_B T \lesssim 25$  and preventing us from reaching the regime where  $T \ll T_K$  throughout the  $N = 1$  state.  $T \ll T_K$  may still be achieved close to the charge transition, however, in the so-called mixed-valence regime where  $\epsilon_0 \lesssim \Gamma$  and the electron is not yet strongly localized in the dot.

In this case, with  $T$  below  $T_K$  near the midpoint of the charge transition, the arrival of the reservoir-hybridized electron in the dot does not immediately bring with it the proportional spin-1/2 entropy contribution that would be expected in the absence of Kondo screening. Instead, the entropy appears once  $T_K$  has been suppressed by a more positive  $V_D \propto \epsilon_0$ , eventually ending in a state where the QD is occupied by a spin-1/2 electron with the expected total entropy change of  $k_B \ln 2$ . Because  $T_K$  increases with  $\Gamma$  for a given  $\epsilon_0$ , the value of  $\epsilon_0$  where  $T_K$  drops below  $T$  also increases with  $\Gamma$ , and the emergence of entropy in the dot is pushed to higher  $\epsilon_0$  for the higher  $\Gamma$  curves.

This suppression of spin entropy due to the Kondo singlet in the mixed-valence regime explains the rightward shift of the rise in  $\Delta S(\epsilon_0)$  at higher  $\Gamma$  in the NRG calculations of Fig. 3c. Pushing the calculations to experimentally unachievable temperatures, it is seen that the rise in  $\Delta S(\mu)$  may be shifted deep into the  $N = 1$  state (data not shown), where the charging energy would become important. In the measurements, no shift in the  $\Delta S(V_D)$  curves is seen: the midpoint  $\Delta S(V_D) = 0.5k_B \ln 2$  stays pinned close to  $\Delta V_D = 0$ , where  $N = 1/2$ .

The evolution of  $S(V_D)$  lineshape from weakly to strongly coupled regimes (Fig. 3a) clearly demonstrates the effect of hybridization on the measured entropy. However, it remains a puzzle why the strong suppression of entropy right at the charge transition, seen in NRG calculations for  $\Gamma/k_B T \geq 5$ , is not observed in the data. It has been suggested [28] that the charge measurement itself can lead to dephasing of the Kondo singlet. Ref. 29 reported a rapid suppression of the Kondo peak in the conductance due to charge sensing. Those results implied significantly stronger dephasing than had been predicted theoretically, and led to new theoretical work proposing alternative dephasing mechanisms. In order to test for charge-sensor dephasing in our measurement, the experiment was repeated at  $V_{CS}$  down to 50  $\mu V$ , but no dependence on  $V_{CS}$  was seen in the data [25]. In the future, experiments that allow simultaneous transport and entropy characterization of the Kondo state may help to resolve this puzzle. We note that the entropy measurement presented here is the first that could be sensitive to the dephasing of the Kondo state itself, rather than dephasing of transport through the Kondo resonance [30].

**ACKNOWLEDGEMENTS:** This project has received funding from European Research Council (ERC) under the European Union's Horizon 2020 research and innovation programme under grant agreement No 951541. Y. Meir acknowledges discussions with A. Georges and support by the Israel Science Foundation (grant 3523/2020).



Experiments at UBC were undertaken with support from the Stewart Blusson Quantum Matter Institute, the Natural Sciences and Engineering Research Council of Canada, the Canada Foundation for Innovation, the Canadian Institute for Advanced Research, and the Canada First Research Excellence Fund, Quantum Materials and Future Technologies Program. SF, GCG. and MM were supported by the US DOE Office of Basic Energy Sciences, Division of Materials Sciences and Engineering award no. DE-SC0006671, with additional support from Nokia Bell Laboratories for the MBE facility gratefully acknowledged.

---

\* [timjchild@gmail.com](mailto:timjchild@gmail.com)

† [jfolk@physics.ubc.ca](mailto:jfolk@physics.ubc.ca)

- [1] Yu Saito, Fangyuan Yang, Jingyuan Ge, Xiaoxue Liu, Takashi Taniguchi, Kenji Watanabe, J. I. A. Li, Erez Berg, and Andrea F. Young, “Isospin Pomeranchuk effect in twisted bilayer graphene,” *Nature* **592**, 220–224 (2021).
- [2] Asaf Rozen, Jeong Min Park, Uri Zondiner, Yuan Cao, Daniel Rodan-Legrain, Takashi Taniguchi, Kenji Watanabe, Yuval Oreg, Ady Stern, Erez Berg, Pablo Jarillo-Herrero, and Shahal Ilani, “Entropic evidence for a Pomeranchuk effect in magic-angle graphene,” *Nature* **592**, 214–219 (2021), 2009.01836.
- [3] Biao Lian, “Heating freezes electrons in twisted bilayer graphene,” *Nature* **592**, 191193 (2021).
- [4] Gilad Ben-Shach, Arbel Haim, Ian Appelbaum, Yuval Oreg, Amir Yacoby, and Bertrand I. Halperin, “Detecting Majorana modes in one-dimensional wires by charge sensing,” *Physical Review B* **91**, 045403 (2015), 1406.5172.
- [5] Eran Sela, Yuval Oreg, Stephan Plugge, Nikolaus Hartman, Silvia Lscher, and Joshua Folk, “Detecting the universal fractional entropy of Majorana zero modes,” *Physical Review Letters* (2019), 10.1103/physrevlett.123.147702, 1905.12237.
- [6] G. Ben-Shach, C. R. Laumann, I. Neder, A. Yacoby, and B. I. Halperin, “Detecting Non-Abelian Anyons by Charging Spectroscopy,” *Physical Review Letters* **110**, 106805 (2013), 1212.1163.
- [7] Nikolaus Hartman, Christian Olsen, Silvia Lscher, Mohammad Samani, Saeed Fallahi, Geoffrey C. Gardner, Michael Manfra, and Joshua Folk, “Direct entropy measurement in a mesoscopic quantum system,” *Nature Physics* **14**, 1083–1086 (2018), 1905.12388.
- [8] Yaakov Kleedorin, Holger Thierschmann, Hartmut Buhmann, Antoine Georges, Laurens W. Molenkamp, and Yigal Meir, “How to measure the entropy of a mesoscopic system via thermoelectric transport,” *Nature Communications* **10**, 5801 (2019), 1904.08948.
- [9] J. M. Elzerman, R. Hanson, L. H. Willems van Beveren, B. Witkamp, L. M. K. Vandersypen, and L. P. Kouwenhoven, “Single-shot read-out of an individual electron spin in a quantum dot,” *Nature* **430**, 431–435 (2004), cond-mat/0411232.
- [10] J. R. Petta, A. C. Johnson, J. M. Taylor, E. A. Laird, A. Yacoby, M. D. Lukin, C. M. Marcus, M. P. Hanson, and A. C. Gossard, “Coherent Manipulation of Coupled Electron Spins in Semiconductor Quantum Dots,” *Science* **309**, 2180–2184 (2005).
- [11] R. Hanson, L. P. Kouwenhoven, J. R. Petta, S. Tarucha, and L. M. K. Vandersypen, *Spins in few-electron quantum dots*, Ph.D. thesis (2007).
- [12] C. Barthel, D. J. Reilly, C. M. Marcus, M. P. Hanson, and A. C. Gossard, “Rapid Single-Shot Measurement of a Singlet-Triplet Qubit,” *Physical Review Letters* **103**, 160503 (2009), 0902.0227.
- [13] Hendrik Bluhm, Sandra Foletti, Diana Mahalu, Vladimir Umansky, and Amir Yacoby, “Enhancing the Coherence of a Spin Qubit by Operating it as a Feedback Loop That Controls its Nuclear Spin Bath,” *Physical Review Letters* **105**, 216803 (2010), 1003.4031.
- [14] K. C. Nowack, M. Shafiei, M. Laforest, G. E. D. K. Prawiroatmodjo, L. R. Schreiber, C. Reichl, W. Wegscheider, and L. M. K. Vandersypen, “Single-Shot Correlations and Two-Qubit Gate of Solid-State Spins,” *Science* **333**, 1269–1272 (2011).
- [15] M. D. Shulman, O. E. Dial, S. P. Harvey, H. Bluhm, V. Umansky, and A. Yacoby, “Demonstration of Entanglement of Electrostatically Coupled Singlet-Triplet Qubits,” *Science* **336**, 202–205 (2012), 1202.1828.
- [16] Eugenia Pyurbeeva and Jan A Mol, “A Thermodynamic Approach to Measuring Entropy in a Few-Electron Nanodevice,” *Entropy* **23**, 640 (2021), 2008.05747.
- [17] D. Goldhaber-Gordon, Hadas Shtrikman, D. Mahalu, David Abusch-Magder, U. Meirav, and M. A. Kastner, “Kondo effect in a single-electron transistor,” *Nature* **391**, 156–159 (1998).
- [18] Michael Pustilnik and Leonid Glazman, “Kondo effect in quantum dots,” *Journal of Physics: Condensed Matter* **16**, R513 (2004), cond-mat/0401517.
- [19] R. M. Potok, I. G. Rau, Hadas Shtrikman, Yuval Oreg, and D. Goldhaber-Gordon, “Observation of the two-channel Kondo effect,” *Nature* **446**, 167–171 (2007), cond-mat/0610721.
- [20] A. J. Keller, L. Peeters, C. P. Moca, I. Weymann, D. Mahalu, V. Umansky, G. Zarnd, and D. Goldhaber-Gordon, “Universal Fermi liquid crossover and quantum criticality in a mesoscopic system,” *Nature* **526**, 237–240 (2015), 1504.07620.
- [21] J. P. Dehollain, U. Mukhopadhyay, V. P. Michal, Y. Wang, B. Wunsch, C. Reichl, W. Wegscheider, M. S. Rudner, E. Demler, and L. M. K. Vandersypen, “Nagaoka ferromagnetism observed in a quantum dot plaquette,” *Nature* **579**, 528–533 (2020), 1904.05680.
- [22] O Legeza, C P Moca, A I Toth, I Weymann, and G Zarand, “Manual for the Flexible DM-NRG code,” arXiv (2008), 0809.3143.
- [23] A. I. Tth, C. P. Moca, . Legeza, and G. Zarnd, “Density matrix numerical renormalization group for non-Abelian symmetries,” *Physical Review B* **78**, 245109 (2008), 0802.4332.
- [24] “Arxiv citation –,” Arxiv.
- [25] “See supplemental material at [url].”.
- [26] Jun Kondo, “Resistance Minimum in Dilute Magnetic Alloys,” *Progress of Theoretical Physics* **32**, 37–49 (1964).
- [27] D. Goldhaber-Gordon, J. Gres, M. A. Kastner, Hadas Shtrikman, D. Mahalu, and U. Meirav, “From the Kondo Regime to the Mixed-Valence Regime in a Single-Electron Transistor,” *Physical Review Letters* **81**, 5225–5228 (1998).

- [28] Alessandro Silva and Shimon Levit, “Peculiarities of the controlled dephasing of a quantum dot in the kondo regime,” *EPL (Europhysics Letters)* **62**, 103 (2003).
  - [29] M Avinun-Kalish, Moty Heiblum, Alessandro Silva, Diana Mahalu, and V Umansky, “Controlled dephasing of a quantum dot in the kondo regime,” *Physical review letters* **92**, 156801 (2004).
  - [30] Kicheon Kang and Gyong Luck Khym, “Entanglement, measurement, and conditional evolution of the kondo singlet interacting with a mesoscopic detector,” *New Journal of Physics* **9**, 121 (2007).
-

## SUPPLEMENTARY MATERIAL

### DEVICE FABRICATION

The device was fabricated in a GaAs/AlGaAs heterostructure that hosts a 2D Electron Gas (2DEG) 57nm below the surface and that had a 300 mK carrier density of  $2.42 \times 10^{11} \text{cm}^{-2}$  with mobility  $2.56 \times 10^6 \text{cm}^2/(\text{Vs})$ . A UV laser writer was used to define the mesas, followed by electron beam lithography to define NiAuGe ohmic contacts. Additionally, 10 nm of  $\text{HfO}_2$  was deposited by atomic layer deposition to improve gating stability. The electrostatic gates were fabricated with two stages of electron beam lithography followed by electron beam evaporation: a fine step for the inner parts, and a coarse step for the outer parts of the gates. In the fine step, 2/12 nm of Pd/Au were deposited. In the coarse step, 10/150 nm of Ti/Au were deposited.

### MEASUREMENT ELECTRONICS

A custom built combined DAC/ADC unit was used to apply potentials to the gates and heating QPCs as well as to record the voltage output of a Current to Voltage Basel SP983c amplifier (<https://www.baspi.ch/low-noise-high-stab-itov-conv>). The DAC/ADC unit is built from an Arduino Due and two Analog Devices evaluations boards: the AD5764 DAC and AD7734 ADC. The Arduino is the interface between the measurement PC and the DAC/ADC boards. The whole design is based on the information provided at [<http://opendacs.com/dac-adc-homepage/>] with some substantial modifications, particularly to the Arduino code (<https://github.com/folk-lab/FastDAC>). The most significant modification is to provide functionality to apply a synchronized square wave bias for heating, whilst measuring continuously.

### CHARGE SENSOR MAPPING

The charge sensor is tuned to the most linear regime before each measurement (Fig. 1a). In the limit of very strong coupling, however, the transition becomes so broad that the non-linearity of the charge sensor may begin to play a role. In our experiment,  $\Delta I_{CS}$  is converted to  $\Delta N$  assuming a linear relation between the two, but when  $I_{CS}$  is not linear in the additional electrostatic potential provided by, e.g., cross capacitance with  $V_D$ , this assumption is no longer valid.

To remove potential inaccuracy in the conversion between  $\Delta I_{CS}$  and  $\Delta N$  due to non-linearity,  $I_{CS}$  may be mapped back to an equivalent charge sensor gate voltage using a measurement  $I_{CS}(V_{QPC})$  (Fig. 1b). Performing the entropy calculation using the equivalent gate voltage, instead of  $I_{CS}$ , significantly reduces any impact of charge sensor non-linearity in the measurement of  $\Delta N$ . In practice, however, no statistically significant difference was observed in entropy calculations using the two approaches, so charge sensor mapping was not used.

### DETERMINING $\Delta S$ BY DIRECT FITTING OF $dN/dT$ DATA

For systems where the addition of an electron to the charge sensed quantum dot has a simple lineshape, as in the case of a QD weakly coupled to a thermal reservoir, it is possible to extract the entropy change of the system by fitting the  $\Delta I_{CS}$  data directly as was done in Hartman et al, Nat Phys 2018. This procedure is made possible through the application of the Maxwell relation:

$$\left( \frac{\partial \mu}{\partial T} \right)_{p,N} = - \left( \frac{\partial S}{\partial N} \right)_{p,T}$$

For a QD weakly coupled to a thermal reservoir, the charging lineshape takes the form:

$$N(V_D, \Theta) = \tanh \left( \frac{V_D - V_{mid}(\Theta)}{2\Theta} \right)$$

where  $\Theta = \frac{k_B T}{\alpha e}$  and  $V_{mid}(\Theta)$  is the plunger gate voltage at  $N = 1/2$ .  $V_{mid}$  changes the quantum dot energy level—that is, the energy required to add an electron to the dot—and therefore maps to the chemical potential  $\mu$  in equilibrium.

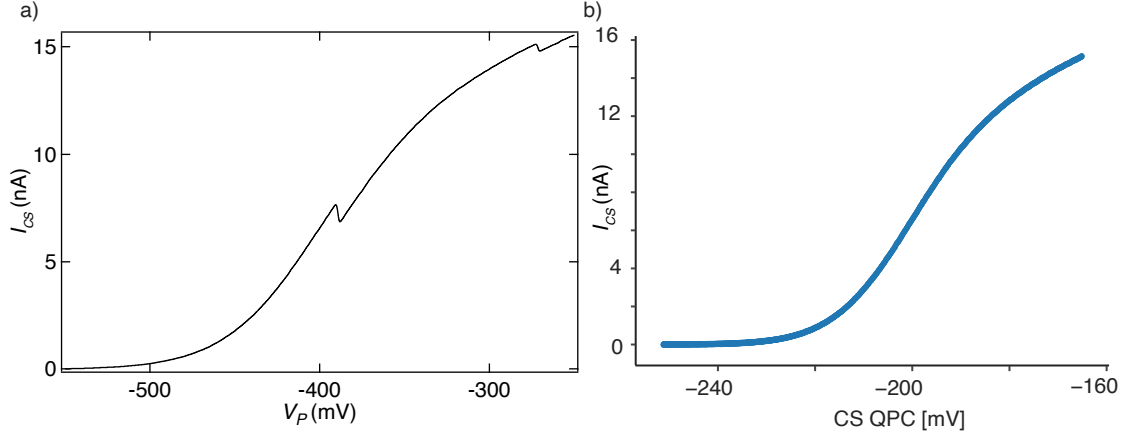


FIG. 1. a) A very wide sweep over a weakly coupled  $0 \rightarrow 1$  transition using the plunger gate showing the response of the charge sensor, and the usual alignment of the  $0 \rightarrow 1$  transition at the steepest, most linear part of the charge sensor response. b) Data of charge sensor current,  $I_{CS}$ , vs the charge sensor QPC tuning gate (see Fig. ??a) used for mapping  $I_{CS}$  to a quantity in units of mV that is linear in electrostatic potential.

Differentiating  $N$  with respect to  $T$ , one finds a lineshape that depends explicitly on  $\Delta S$ :

$$\partial N(V_D, \Theta) \propto -\partial T \left[ \frac{V_D - V_{mid}(\Theta)}{2\Theta} - \frac{\Delta S}{2k_B} \right] \times \cosh^{-2} \left( \frac{V_D - V_{mid}(\Theta)}{2\Theta} \right)$$

after substituting

$$\frac{\partial V_{mid}}{\partial \Theta} = \frac{1}{k_B} \frac{\partial \mu}{\partial T} = \frac{1}{k_B} \Delta S_{N-1 \rightarrow N}$$

Here  $\partial N(V_D, \Theta)$  is the difference in occupation of the QD for the reservoir temperature changing from  $T \rightarrow T + \Delta T$ . Fitting this equation to the  $\Delta I_{CS}$  data,  $\Delta S$  is obtained as a fit parameter independent of the scaling of the data.

## FITTING NRG TO DATA

Our procedure for fitting the occupation,  $N$ , of NRG calculations to measured data involves three steps: 1. Linearly interpolating over the 2D array of calculations. 2. Adding terms (amplitude, constant, linear) to account for the behaviour of the charge sensor in detecting the QD occupations. 3. Allowing for an offset and scaling proportional to  $\Theta$  ( $T$  in units of gate voltage) in the  $\epsilon_0$  axis. We then use Powell's method of minimization to find the best fitting parameters allowing all to vary with the exception of  $\Gamma$  and  $\Theta$ , for which only one is allowed to vary. In the weakly coupled regime, it is reasonable to approximate  $\Gamma \sim 0$ , and with that constraint, we are able to determine  $\Theta(V_D)$ . We find a linear relationship between  $\Theta(V_D)$  and  $V_T$  which implies a linearly changing lever arm,  $\alpha$ , as the system temperature,  $T$ , is fixed. Note that the lever arm,  $\alpha$ , connects  $\Theta$  in units of gate voltage to temperature,  $T$ , in kelvin (Eq.1),

$$\alpha\Theta = k_B T \quad (1)$$

and is a measure of the strength of effect the plunger gate,  $V_D$ , has on the QD. The linear change implies that as  $V_T$  is varied, the strength of effect of  $V_D$  also varies. We attribute this to a change of shape of the QD where it moves it further from  $V_D$  for more positive  $V_T$ . For measurements into the strongly coupled regime where  $\Gamma \gg 0$ , we force the  $\Theta$  parameter to follow the linear relationship found in the weakly coupled regime, allowing  $\Gamma$  to be a varying parameter. The fit parameters found by comparing  $N$  of NRG data to  $I_{CS}$  of measured data can then be used to directly compare between the NRG  $dN/dT$  calculations and  $\Delta I_{CS}$  measurements.



## SCALING FROM $\Delta I_{CS}$ TO $dN/dT$

The complete procedure for scaling from  $\Delta I_{CS}$  to  $dN/dT$  is comprised of two parts: Conversion of  $\Delta I_{CS}$  to  $\Delta N$ , and calculation of the corresponding  $\Delta T$ , expressed in equivalent mV on  $V_D$ .

The procedure for scaling the  $\Delta I_{CS}$  measurements to  $dN/dT$  involves scaling  $\Delta I_{CS} \rightarrow \Delta N$ , then dividing by  $\Delta T$  as described in the main text. The  $\Delta I_{CS} \rightarrow \Delta N$  conversion is a straightforward division by  $I_e$ , the net change of current through the charge sensor for the addition of 1 full electron to the QD. Extracting  $I_e$  from the data is achieved by scaling NRG calculations of occupation across the transition to the heated portion of  $I_{CS}$  data, with additional offset and linear terms added to the NRG to account for cross capacitance between  $V_D$  and the charge sensor.

$\Delta T$  is easily extracted in units of equivalent gate voltage ( $V_D$ ) for weakly coupled  $V_T$  by fitting cold and hot occupation data to NRG. For strongly coupled transitions, however,  $\Delta T$  does not result in a broadening of the transition lineshape, so it must be determined in another way. The real temperature change of the reservoir does not depend on  $V_T$ , of course, but the lever arm  $\alpha$  does depend on  $V_T$ . We calculate  $\Delta T(V_T)$  in equivalent mV on  $V_D$  by

1. fitting hot and cold transitions for a range of weakly coupled  $V_T$ , to determine both  $\Delta T(V_T)$  in equivalent  $V_D$  and  $\alpha(V_T)$  through this range.
2.  $\alpha(V_T)$  is observed to be linear in  $V_T$ , and extrapolated to strongly-coupled  $V_T$  (dashed line in Fig. ??c, main text).
3.  $\Delta T$  in equivalent  $V_D$  is calculated for strongly coupled transitions using  $\alpha(V_T)$  determined above.

## AVERAGING PROCEDURE

The data shown in the main text is the result of averaging measurements over many sweeps over the transition. In the strongly coupled regime, as the  $\Delta I_{CS}$  signal becomes weaker, averaging data becomes particularly important. It is often necessary to measure for 10's of minutes or even hours in order to obtain a reasonable signal to noise ratio, but the presence of charge instability makes single slow measurements over the transition unreliable. By repeatedly sweeping over the transition quickly, then aligning each sweep based on a fit to the  $I_{CS}$  data before averaging, we can improve the signal to noise ratio of the corresponding  $\Delta I_{CS}$  whilst mitigating the effect of charge instability. This procedure of post-aligning individual charge transition scans is followed for measurements in the range  $V_T < -230$  mV.

For more strongly coupled measurements ( $V_T \geq -230$  mV), determining the center of each individual scan through fitting is not reliable; as a result, data is averaged without centring first. Charge instability (determined in the weakly coupled regime) is on the order of  $6 \mu\text{eV}$  without significant long-term drift seen in the data. For the most strongly coupled measurements, where the width of the transition is on the order of  $400 \mu\text{eV}$ , the lack of centring therefore is expected to have a negligible effect. Occasional larger jumps in transition position ( $0.5$  mV) do occur on a timescale of hours; care is taken never to average data across such jumps.

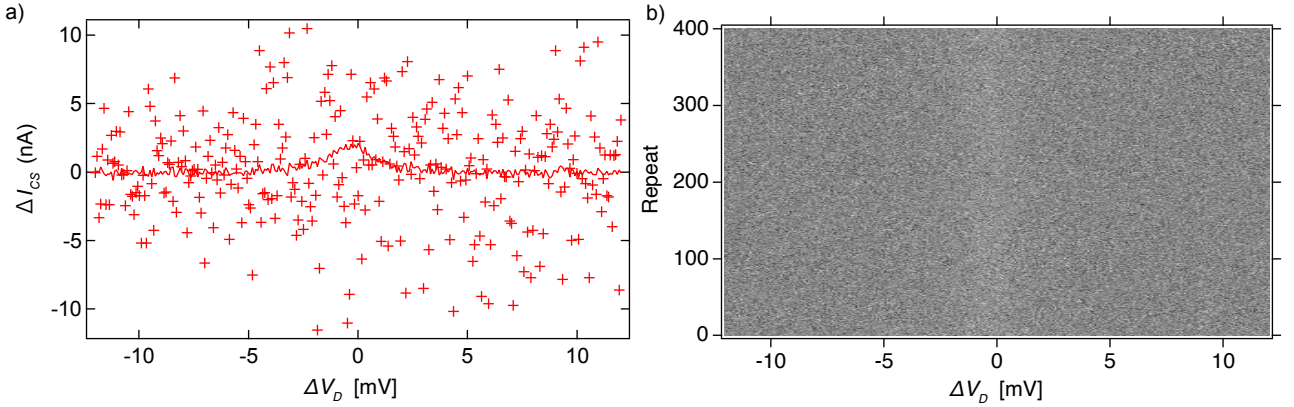


FIG. 2. a) Markers illustrate a single measurement across the charge transition, which takes 30 seconds to complete. No peak in  $\Delta I_{CS}$  can be seen in this raw data. After averaging 400 of such scans together (solid line), however, a small peak in  $\Delta I_{CS}$  is seen at  $\Delta V_D = 0$ . b) Raw  $\Delta I_{CS}$  data (greyscale) for 400 scans as in panel a). Averaged together, they yield the solid line in panel a).

# LACK OF DEPENDENCE ON CHARGE SENSOR BIAS

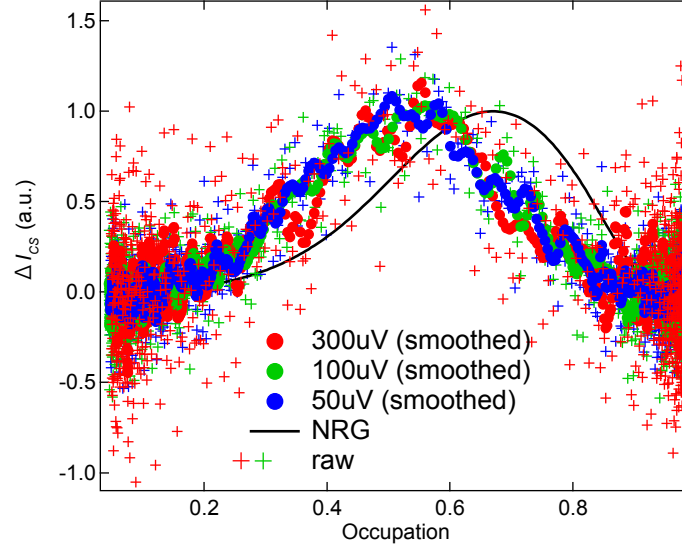


FIG. 3. The lineshape of  $\Delta I_{CS}$ , here plotted vs occupation instead of  $V_D$ , shows no dependence on  $V_{CS}$  within experimental noise, though of course the magnitude of  $I_{CS}$  and  $\Delta I_{CS}$  scales linearly with  $V_{CS}$ . The case of  $\Gamma/k_B T = 24$  is shown here. In particular,  $\Delta I_{CS}$  remains peaked at  $N \sim 0.5$ , in contrast to the NRG calculation (solid line) in which the shifted peak reflects the screening of spin entropy in the mixed valence regime due to the formation of the Kondo singlet.